Journal of Power Sources 247 (2014) 314–321

Contents lists available at ScienceDirect

Journal of Power Sources

journal homepage: www.elsevier.com/locate/jpowsour

Impedance spectroscopy of the oxide films formed during high temperature oxidation of a cobalt-plated ferritic alloy

S. Velraj [a], J.H. Zhu [a, b, *], A.S. Painter [a], S.W. Du [b], Y.T. Li [b]

[a] Department of Mechanical Engineering, Tennessee Technological University, Box 5014, Cookeville, TN 38501, USA
[b] School of Materials Science and Engineering, Taiyuan University of Science and Technology, Taiyuan 030024, China

HIGHLIGHTS

- Co plating was used to synthesize the spinel coating on a ferritic steel.
- Impedance spectroscopy was used to characterize the oxide layers after oxidation.
- Two layers of oxides (Co_3O_4 and Cr_2O_3) were observed for the 2-h sample.
- An additional $CoCr_2O_4$ layer was identified for the 50-, 100-, and 500-h samples.

ARTICLE INFO

Article history:
Received 8 July 2013
Received in revised form
23 August 2013
Accepted 26 August 2013
Available online 5 September 2013

Keywords:
Solid oxide fuel cell
Interconnect
Spinel
Impedance spectroscopy
Cobalt plating
Oxide scale

ABSTRACT

Impedance spectroscopy was used to evaluate the oxide films formed on cobalt-coated Crofer 22 APU ferritic stainless steel after thermal oxidation at 800 °C in air for different times (i.e. 2, 50, 100 and 500 h). Impedance spectra of the oxide films exhibited two or three semicircles depending on the oxidation time, which correspond to the presence of two or three individual oxide layers. Coupled with scanning electron microscopy/energy-dispersive spectroscopy (SEM/EDS) and X-ray diffraction (XRD), the individual oxide layer corresponding to each semicircle was determined unambiguously. Impedance spectrum analysis of the oxide films formed on the sample after thermal exposure at 800 °C in air for 2 h led to the identification of the low-frequency and high-frequency semicircles as being from Cr_2O_3 and Co_3O_4, respectively. SEM/EDS and XRD analysis of the 500-h sample clearly revealed the presence of three oxide layers, analyzed to be $Co_{3-x}Cr_xO_4$, $CoCr_2O_4$, and Cr_2O_3. Although the SEM images of the 50-h and 100-h samples did not clearly show the $CoCr_2O_4$ layer, impedance plots implied their presence. The oxide scales were assigned to their respective semicircles and the electrical properties of $Co_{3-x}Cr_xO_4$, $CoCr_2O_4$ and Cr_2O_3 were determined from the impedance data.

1. Introduction

Solid oxide fuel cell (SOFC) is a promising electrochemical energy conversion technology for green power generation. The advantages of SOFC include high efficiency, fuel flexibility, environmental friendliness, etc. Nevertheless, this kind of fuel cell has to face an important challenge; the operating temperature is around 800–1000 °C, resulting in the need of components (cathode, anode, electrolyte and interconnect) sustaining severe operating conditions [1]. Ceramic materials used as interconnect are expensive and difficult to machine. Recent developments have lowered the SOFC stack operating temperature to around 600–800 °C, paving the way for the use of stainless steel as interconnect material and thus significantly reducing the stack cost [2,3]. Among various steels, ferritic stainless steels have gained the most attention due to their close match in coefficient of thermal expansion (CTE) with ceramic components used in SOFC [4]. High-temperature oxidation and corrosion process, which occurs for all metallic alloys exposed to SOFC operating conditions, results in oxide scale formation and growth on the alloy surface. The oxide scale can have low electronic conductivity, unmatched CTE with the interconnect steel and cell components, or detrimental reaction with ceramic functional layers. Generally, only chromia (Cr_2O_3) is regarded as prospective oxide scale [5], as it has a relatively high electrical conductivity in comparison to other possible protective scales such as Al_2O_3 and SiO_2 [3,6]. However, Cr_2O_3-forming alloys

* Corresponding author. Department of Mechanical Engineering, Tennessee Technological University, Box 5014, Cookeville, TN 38501, USA. Tel.: +1 931 372 3186; fax: +1 931 372 6340.
E-mail address: jzhu@tntech.edu (J.H. Zhu).

0378-7753/$ – see front matter © 2013 Elsevier B.V. All rights reserved.
http://dx.doi.org/10.1016/j.jpowsour.2013.08.120

suffer from Cr volatilization. The volatile Cr species could migrate to and poison the cathode, resulting in drastically reduced cathode activity and subsequent degradation of the SOFC performance [7–9]. A significant amount of research efforts has been conducted to address this issue by either the design of new spinel-forming alloys or the development of surface coatings that are electrically-conductive and Cr-blocking.

In spite of the extensive spinel-forming alloy development, the path to low-cost high-performance metallic interconnect is incomplete. Crofer 22 APU, a Cr_2O_3-forming ferritic steel, forms a double-layer surface oxide structure with a $(Cr,Mn)_3O_4$ spinel outer layer atop a Cr_2O_3 inner layer [10]. Cr evaporation from this alloy is significantly reduced by the formation of the thermally-grown spinel surface layer. However, the $(Cr,Mn)_3O_4$ spinel has relatively low conductivity and does not prevent the continuous growth of the subscale Cr_2O_3, which can lead to scale thickening and eventual spallation after long-term exposure. Furthermore, Cr evaporation is not fully mitigated due to the presence of Cr in this spinel. Electrically-conductive and Cr-blocking spinel coatings have also been studied as an alternative approach. Spinel coatings such as Co_3O_4, $(Co,Mn)_3O_4$ and $CoFe_2O_4$ over Crofer 22 APU interconnect have been shown to reduce the growth rate of the native Cr_2O_3 scale, while also acting as a physical barrier to Cr evaporation, thereby improving the long-term performance stability of the SOFC stack [11–13]. The interdiffusion between the Co_3O_4 coating and the oxide scales formed at high temperature on various ferritic steels including Crofer 22 APU have been evaluated along with their scale area specific resistance (ASR) [14–19]. The Co_3O_4 layer has been shown to reduce the overall degradation rate and lower the scale ASR. Larring et al. reported the lowest degradation rate for the Co_3O_4 coating in comparison with various perovskites (e.g. $LaCrO_3$ and $(La,Sr)CoO_3$) and spinels (e.g. Mn_3O_4) [19]. Hansson et al. suggested that the results obtained by Larring et al. could be due to a higher electrical conducting oxide scale rather than a protective scale that reduced the Cr oxidation rate [16].

It is important to understand the interaction of the Co_3O_4 coating with thermally-grown oxide scales, their electrical properties and potential consumption of the Co_3O_4 coating during long-term SOFC operation. Impedance spectroscopy, a non-destructive technique, can be used to assess the presence, growth, and

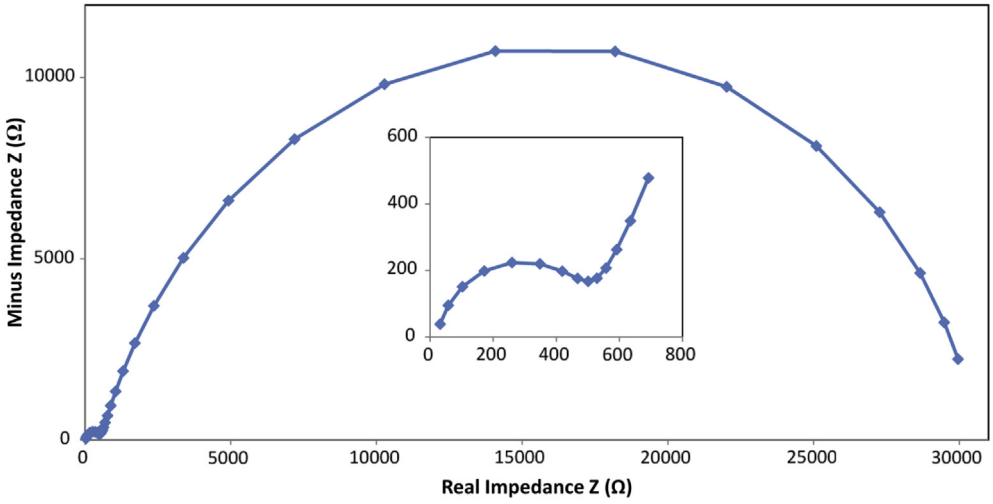

(a)

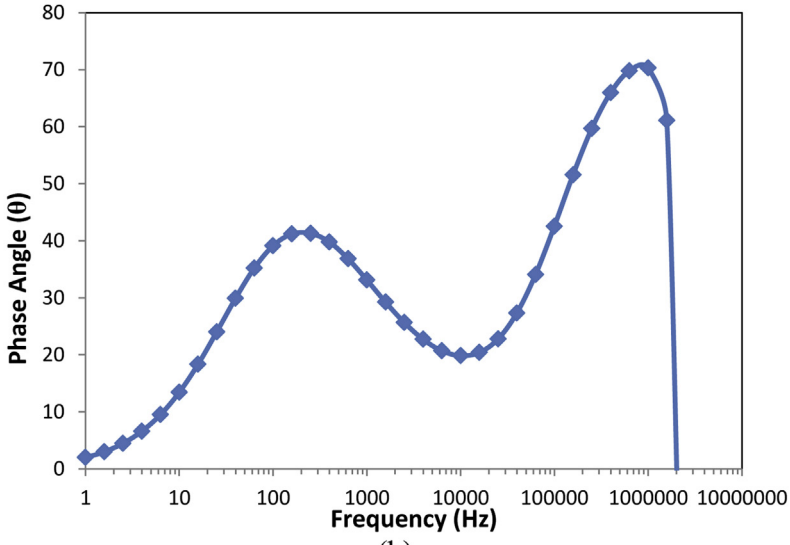

(b)

Fig. 1. (a) Nyquist plot with an inset showing the high-frequency-range part and (b) Bode plot for the cobalt-plated sample after oxidation at 800 °C in air for 2 h.

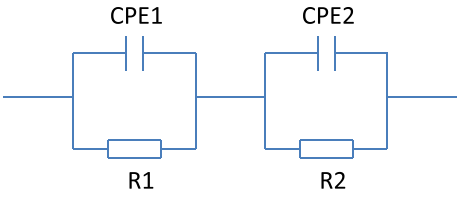

Fig. 2. A typical equivalent circuit of two *R*–*C* components with a series connection used to fit the impedance spectrum with two oxide layers.

electrical properties of each individual oxide scale. In this study, the effect of the Co_3O_4 layer on the growth of other oxide scales on Crofer 22 APU during high temperature oxidation is investigated using impedance spectroscopy. The electrical properties of the various oxide layers formed during oxidation are also determined.

2. Experimental

The electroplating solution was prepared by dissolving 150-g $CoSO_4 \cdot 7H_2O$ and 25-g $CoCl_2 \cdot 6H_2O$ in 500-g distilled water, followed by the addition of 15-g H_3BO_3 to the solution. The material used in this study was 1.0 mm Crofer 22 APU sheet supplied by ThyssenKrupp, with a batch chemical composition (in wt%) of 22% Cr, 0.45% Mn, 0.06% La, 0.1% Si, 0.12% Al, 0.005% C, 0.08% Ti, balance Fe. The sheet was cut into coupons of 12 mm × 12 mm square, cleaned ultrasonically in deionized water and acetone, and then etched for 2 min in a 10% H_2SO_4 solution. The Crofer 22 APU substrate was used as the cathode while two pure cobalt plates were used as the anode. Cobalt electroplating was conducted at a current density of 22 mA cm^{-2} for 5 min, resulting in a cobalt layer of ~2.5 μm in thickness. The cobalt-coated coupons were then oxidized at 800 °C in air for various durations (i.e. 2, 50, 100 and 500 h). Subsequently, silver paste was painted on one side of the sample in a circle of 8 mm in diameter and cured at 800 °C for 0.5 h, which served as one electrode. Finally, the oxide scale on the other side was polished off and the exposed metal served as the other electrode.

Impedance measurements were made using a Solartron SI 125 HF frequency response analyzer equipped with a Solartron 1296 dielectric interface. In the measurements, an AC amplitude of 0.1 V was applied to the sample with the AC frequency in the range of 1 to 1×10^6 Hz. Impedance measurements were performed at room temperature. Spectra analysis was carried out using the Zview impedance analysis software to extract electrical properties of the oxide films.

Scanning electron microscopy (FEI Quanta 200 FEG) attached with energy-dispersive spectroscopy (SEM/EDS) was employed to characterize the microstructural features and compositional information of the oxide films. The crystal structures of the oxide films were determined by X-ray diffraction (XRD; Rigaku Ultima IV) using Cu Kα radiation. Since the information depth of the XRD measurements is only a few micrometers for the oxides, the oxide scales underneath the Co_3O_4 layer may not be detected. To reveal and identify the other oxide scales, the surface spinel layer of the 500-h sample was carefully polished off and XRD analysis was undertaken on the exposed oxide scales.

3. Results and discussion

3.1. Identification of the oxide layers formed after 2-h oxidation

There are generally two types of impedance diagrams, namely Nyquist plots and Bode plots. In a Nyquist plot, the impedance is represented by a real part and an imaginary part. Therefore, the Nyquist plot is also termed the complex plane impedance plot. In a Bode plot, the modulus of the impedance and the phase angle are both plotted as a function of frequency. For a simple resistor–capacitor (*R*–*C*) circuit, the Nyquist plot is characterized by a semicircle. Usually, the Nyquist plot is used to directly determine the major parameters, such as resistance and capacitance corresponding to an ideal system. For the oxide scale system encountered in this study, the measured oxide system is often not ideal and does not behave as a pure capacitor due to the porosity, surface roughness, and thickness/composition non-uniformity of the oxide layer. This deviation may be accommodated by the use of a constant-phase element (CPE) for spectra fitting instead of an ideal capacitance element. The impedance of a CPE (Z_{CPE}) is given by the following equation [20]:

$$Z_{CPE} = \frac{1}{A(j\omega)^n} \quad (1)$$

where A is a fit parameter independent of frequency $j = \sqrt{-1}$, ω is the radial frequency, and n is the exponential factor. In an ideal case where $n = 1$, the CPE functions as a pure capacitor with A equal to the capacitance C. In most cases, though, the value of n is less than 1. Therefore, the fitted curves are represented by A and n, and the value for the capacitance C can be calculated with the following equation [22]:

$$C = R^{\frac{(1-n)}{n}} A^{\frac{1}{n}} \quad (2)$$

where R is the observed resistance.

Nyquist and Bode plots for the cobalt-plated Crofer 22 APU sample after oxidation at 800 °C in air for 2 h (i.e. 2-h sample) are given in Fig. 1. Obviously, there are two semicircles on the Nyquist plot (Fig. 1a) and two relaxation frequencies on the Bode plot (Fig. 1b), respectively, indicating that two individual oxide layers were formed by thermal oxidation in air for 2 h. Since there are two semicircles present in the impedance spectrum, the spectrum was fitted with an equivalent circuit of two *R*–*C* components with a series connection, as shown schematically in Fig. 2. The values of *R*, *A*, and *n* were obtained from the fitting of each semicircle. The capacitance C was then calculated using Eq. (2). The resistance and capacitance corresponding to each of the two semicircles as well as the relaxation frequency f_R values are shown in Table 1.

The XRD pattern of the 2-h sample reveals the presence of a predominantly Co_3O_4 phase with traces of Cr_2O_3 present, as shown in Fig. 3a. The SEM cross-sectional image of this sample shows a thicker Co_3O_4 layer atop a thinner Cr_2O_3 inner layer, Fig. 4a. The Cr content in the surface Co_3O_4 layer was negligible according to the EDS analysis, due to the short exposure time. Based on these results, the two semicircles in the impedance spectrum of this sample are attributed to the presence of two oxide layers of Co_3O_4 and Cr_2O_3.

Table 1
Resistance and capacitance values of the oxide films formed on the cobalt-plated Crofer 22 APU steel after oxidation at 800 °C for 2 h.

Coating time (min)	Resistance (*R*) (Ω)		Capacitance (*C*) (Fm^{-1})	
	Low-frequency ($f_R = 2.5 \times 10^2$ Hz)	High-frequency ($f_R = 1 \times 10^7$ Hz)	Low-frequency ($f_R = 2.5 \times 10^2$ Hz)	High-frequency ($f_R = 1 \times 10^7$ Hz)
5	30,613	593	2.49×10^{-7}	1.51×10^{-9}

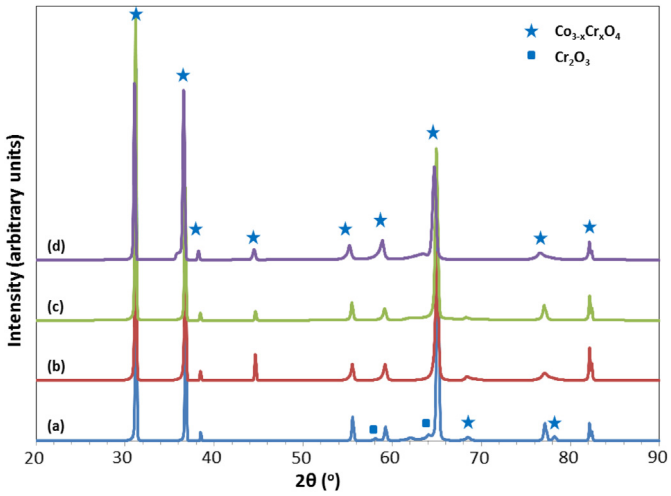

Fig. 3. XRD patterns of the cobalt-plated samples after oxidation at 800 °C in air for different times: (a) 2 h; (b) 50 h; (c) 100 h; and (d) 500 h.

According to Table 1, the capacitance of the low-frequency (LF) semicircle is much higher than that of the high-frequency (HF) semicircle. Since the relative permissivity for Co_3O_4 (i.e. 9.2) and Cr_2O_3 (i.e. 9.59) are close to each other [21], their capacitance must be inversely proportional to the layer thickness. As such, the oxide scale corresponding to LF should be much thinner than that for the HF semicircle. Therefore, coupled with the SEM results in Fig. 4a, it can be concluded that the LF semicircle is related to the thin Cr_2O_3 layer while the HF one is from the much thicker Co_3O_4 layer. The relaxation frequency f_R is a material property at a given temperature and independent of the oxide layer geometry and can also be used to identify the material [20]. The value of f_R for the LF semicircle is 2.5×10^2 Hz (Table 1), which is in good agreement with the available literature data for Cr_2O_3 ($f_R = 2 \times 10^2$ Hz) [23].

The resistivity (ρ) for the oxide scales can be determined from the measured R using $\rho = RA/l$, where A is the contact area (5×10^{-5} m^2) and l is the thickness of the oxide scale as measured by SEM. The calculated resistivity for the Co_3O_4 and Cr_2O_3 layers at room temperature is 6.85×10^3 and 3.0×10^6 Ω m, respectively. These values are in the similar ranges of those reported for Co_3O_4 (i.e. 10^4 Ω m [24]) and Cr_2O_3 (i.e. 10^6 Ω m [21]), which further confirms that our assignments of the two oxides responsible for the two semicircles are reasonable for the 2-h sample.

3.2. Identification of the oxide layers formed after longer oxidation times

The XRD patterns of the cobalt-coated samples after oxidation for various durations are shown in Fig. 3. While as mentioned earlier the 2-h sample indicated the presence of predominantly the

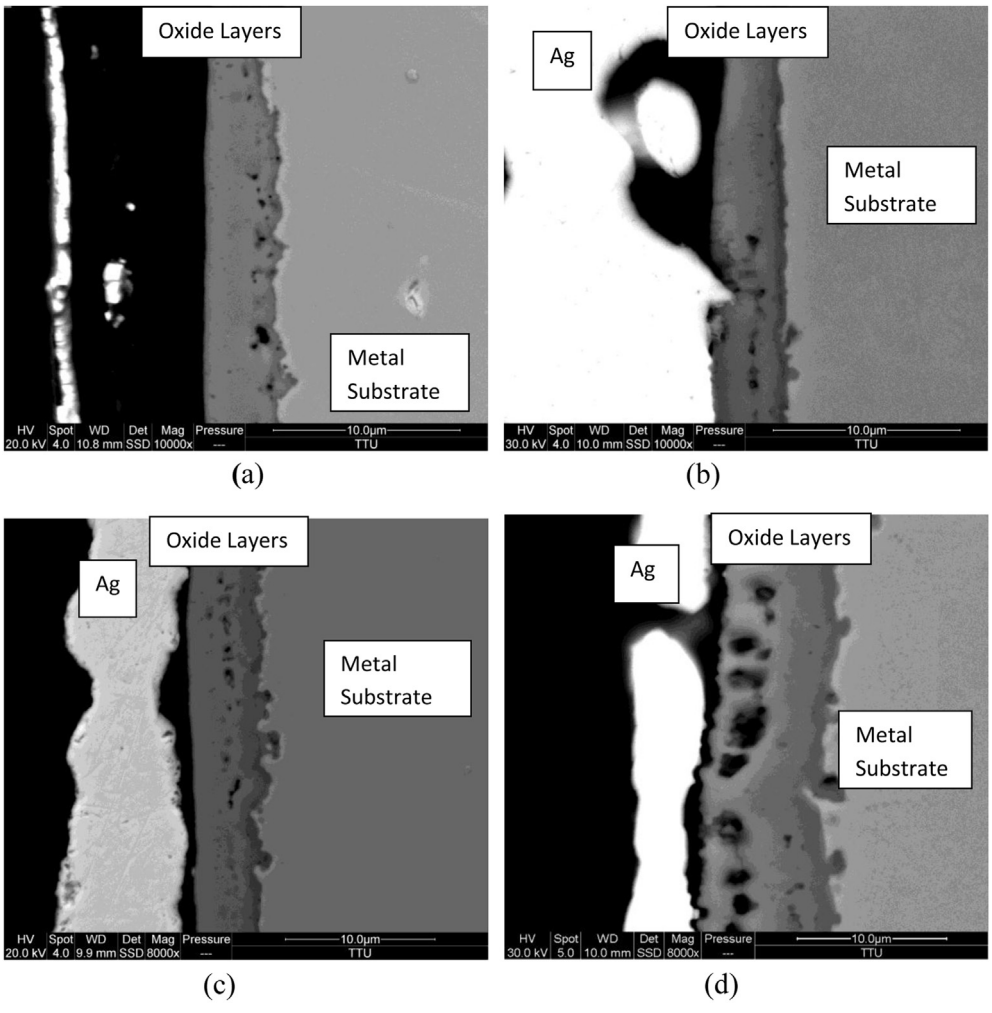

Fig. 4. Cross-sectional images of the cobalt-plated samples after oxidation at 800 °C in air for different times: (a) 2 h; (b) 50 h; (c) 100 h; and (d) 500 h.

Co_3O_4 phase with a small amount of Cr_2O_3, only the spinel phase could be observed for the 50-, 100-, and 500-h samples. A careful examination of the XRD peaks for different samples reveals that as the oxidation time increased the spinel peak positions shifted to the lower 2θ values gradually. It has been reported that Cr can be dissolved in Co_3O_4 to form a single-phase spinel $Co_{3-x}Cr_xO_4$, where $x = 0–2$; furthermore, as x increases in $Co_{3-x}Cr_xO_4$, its lattice parameter increases linearly [25]. Table 2 lists the lattice parameter and the estimated Cr content (i.e. x in $Co_{3-x}Cr_xO_4$) for the surface spinel layer after oxidation for different times. The lattice parameter was determined from the XRD spectra, while the Cr content x was calculated using the O'Neill equation given in Ref. [25]. Clearly, as the oxidation time increased both the lattice parameter of and the Cr content in the $Co_{3-x}Cr_xO_4$ spinel increased, as a result of the cation interdiffusion. It should be noted that the lattice parameter and Cr content given in Table 2 are the apparent values, since the $Co_{3-x}Cr_xO_4$ layer had a Cr concentration gradient and the corresponding XRD peaks were broadened as a result.

As mentioned earlier, since the information depth of XRD is only a few micrometers, any oxide layer beneath the surface spinel layer might not be identified. A cross-sectional SEM image was used to identify the presence and thickness of the individual oxide layers. It appears from Fig. 4a–c that two oxide layers were present without significant change in oxide thickness. Interestingly, a third oxide layer was unambiguously observed between the surface $Co_{3-x}Cr_xO_4$ layer and the inner Cr_2O_3 scale for the 500-h sample (Fig. 4d). EDS analysis indicates that this layer contained a significant amount of Cr. From an analysis of the XRD peaks obtained by polishing off the surface layer of the 500-h sample, this intermediate layer could be identified as the $CoCr_2O_4$ spinel (Fig. 5). Combining the SEM/EDS and XRD results, it is concluded that this layer has a composition corresponding to $CoCr_2O_4$, while the surface spinel is $Co_{3-x}Cr_xO_4$ with varying amounts of Cr contents at different locations. Oxidation studies of cobalt coating on several alloys have also revealed the formation of a $(Co,Cr)_3O_4$ and/or $CoCr_2O_4$ spinel layer due to the oxidation of Co metal and its reaction with the diffusing Cr species [16–19]. Illustrative sketches are shown in Fig. 6, which summarizes the features of the oxide structures formed at different stages. After 2-h oxidation at 800 °C in air, a two-layer structure with a thin inner Cr_2O_3 scale and a surface Co_3O_4 layer essentially free of Cr was developed, Fig. 6a. After oxidation for 50–500 h, a three-layer structure was formed, i.e., Cr_2O_3, $CoCr_2O_4$, and Cr-containing $Co_{3-x}Cr_xO_4$ from the interior to the surface, Fig. 6b,c. As the oxidation time increased, the thickness of the $CoCr_2O_4$ layer increased correspondingly and more Kirkendall voids in the $Co_{3-x}Cr_xO_4$ surface layer were present.

Nyquist plots and Bode plots measured for the samples with different oxidation times are shown in Figs. 7 and 8, in addition to Fig. 1. It can be seen that except for the 2-h sample which had only two semicircles with two relaxation frequencies (Fig. 1), all the other samples exhibited an extra semicircle and relaxation frequencies. Since those two semicircles have been previously identified, this extra semicircle at the lowest frequencies should correspond to the $CoCr_2O_4$ layer. Owing to the fact that three

Table 2
Lattice parameter and the estimated Cr content (x) of the $Co_{3-x}Cr_xO_4$ layer formed on the cobalt-plated Crofer 22 APU steel after oxidation at 800 °C in air for different times.

Oxidation time (h)	Lattice parameter (Å)	Calculated Cr content, x
2	8.0862	0.02
50	8.1024	0.14
100	8.1108	0.21
500	8.1330	0.38

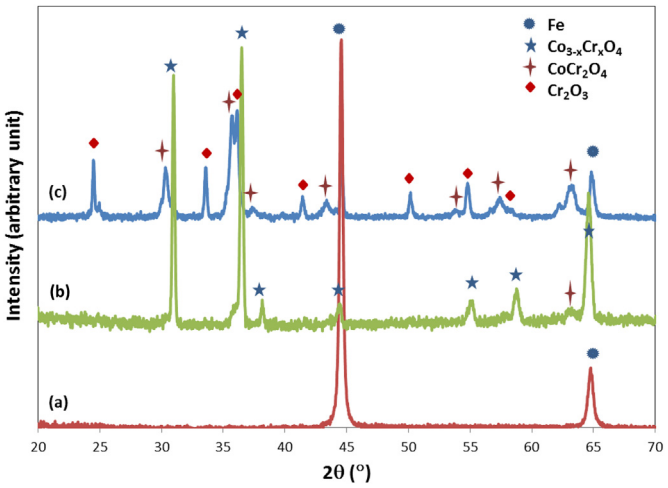

Fig. 5. XRD pattern of the 500-h sample: (a) the oxide scale completely removed to expose the substrate metal, (b) the oxide scale surface unprocessed, and (c) the oxide scale ground to remove the $Co_{3-x}Cr_xO_4$ layer.

semicircles are present in the impedance spectra for the samples after longer oxidation times (>2 h), the spectra were fitted with an equivalent circuit of three R–C components with a series connection similar to those shown in Fig. 2. The relaxation frequency peaks (around 2–10 Hz, Fig. 8) corresponding to the extra semicircle were not very prominent, as there is a range of composition/thickness for this layer at different locations. Similar features were also observed for the relaxation frequency of the surface $Co_{3-x}Cr_xO_4$ layer, especially after 500-h oxidation. These results are consistent with the observed XRD peak broadening as is clear from Figs. 3 and 5, indicative of the presence of a compositional range for both spinel layers. The electrical resistivity of the $CoCr_2O_4$ spinel layer calculated using the data obtained from the 500-h sample was 2.7×10^7 Ω m at room temperature. From the data reported by W. Qu et al. [26], the room temperature resistivity of $CoCr_2O_4$ was estimated to be about 3.2×10^6 Ω m. Hence, the measured resistivity may be influenced by the composition/thickness variation of the spinel as mentioned earlier. It should be noted that the

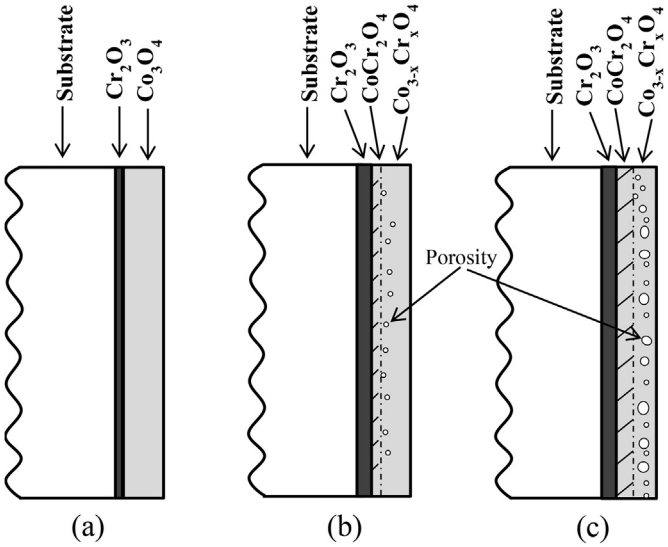

Fig. 6. Sketches illustrating the features of the oxide structures formed after oxidation at 800 °C in air for different times: (a) 2 h; (b) 50/100 h; and (d) 500 h.

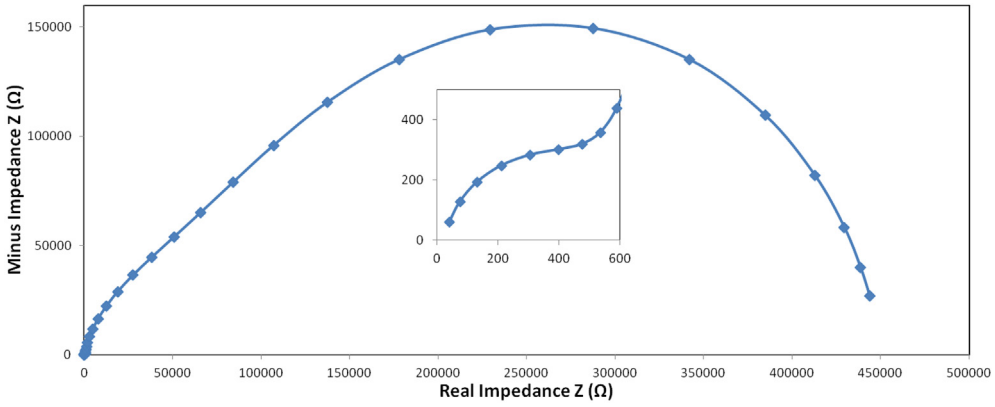

(a)

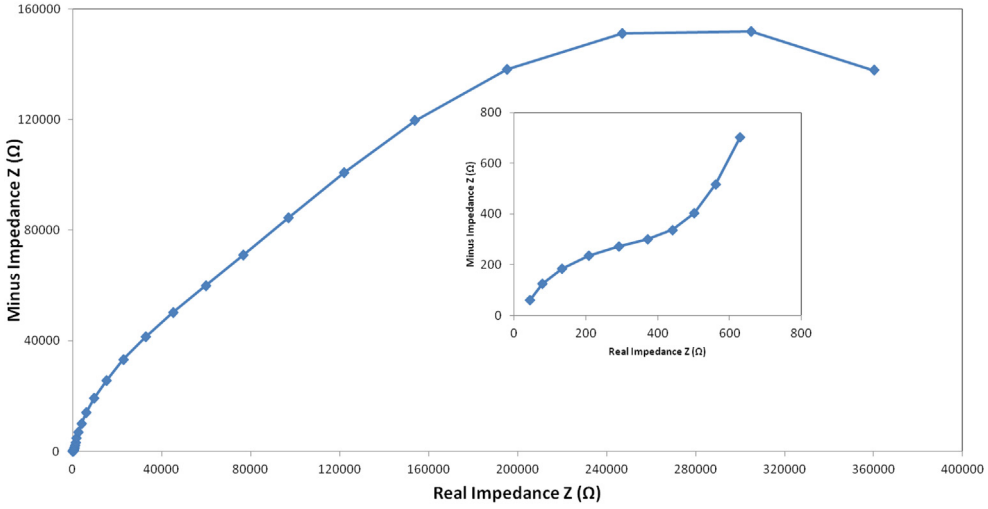

(b)

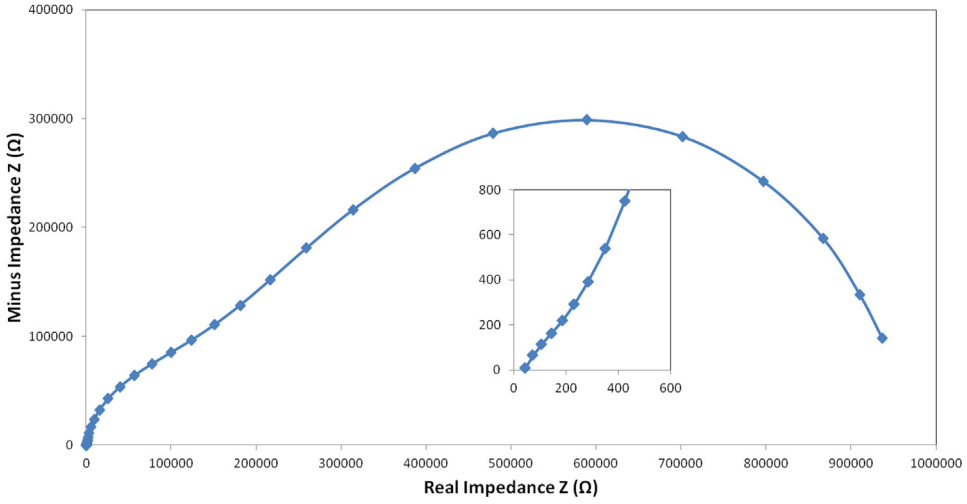

(c)

Fig. 7. Nyquist plots obtained for the cobalt-plated samples after oxidation at 800 °C for different times, with insets showing the high-frequency-range parts: (a) 50 h; (b) 100 h; and (c) 500 h.

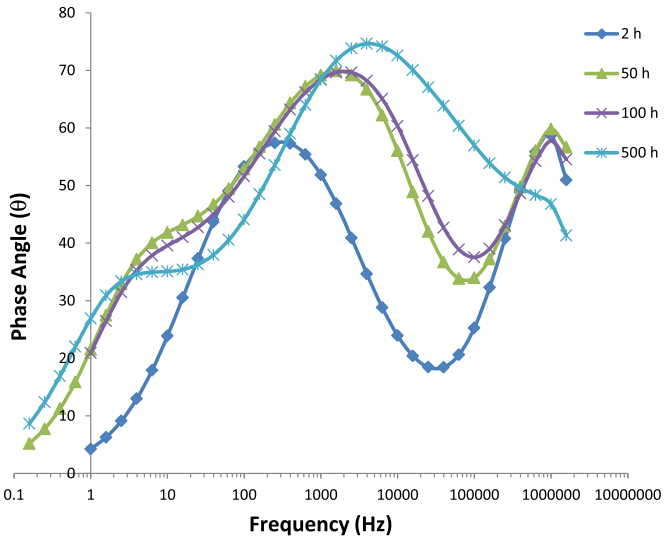

Fig. 8. Bode plots obtained for the cobalt-plated samples after oxidation at 800 °C for different times.

relaxation frequency corresponding to the Cr_2O_3 layer increased from 250 Hz for the 2-h sample to about 3000 Hz for the 500-h sample. This might be a result of incorporation of Fe and Mn into Cr_2O_3, which diffused from the substrate after extended thermal exposures [14].

The resistance of the Cr_2O_3 and $CoCr_2O_4$ layers increased as a function of oxidation time while the resistance of $Co_{3-x}Cr_xO_4$ decreased correspondingly (Fig. 9). Similarly, the capacitance of the Cr_2O_3 and $CoCr_2O_4$ layers increased as a function of oxidation time while the capacitance of the $Co_{3-x}Cr_xO_4$ layer decreased (Fig. 10). This could be due to the diffusion of Co from $Co_{3-x}Cr_xO_4$ to facilitate the growth of the $CoCr_2O_4$ while Cr is supplied by the metal substrate to feed the thickening of the Cr_2O_3 layer. Evidence of the cobalt loss from the surface spinel layer is the presence of Kirkendall voids in the 500-h sample, as shown in Fig. 4d as well as illustrated in Fig. 6c. The formation of these voids is detrimental to the electrical conduction in the interconnect alloy/coating, which will be a serious issue for such Co_3O_4 spinel-based system during long-term SOFC stack operation. Interactions between the Cr_2O_3 scale and the Co_3O_4 surface layer need to be minimized for improving the coating performance stability, which might be achieved via doping of transition-metal cations such as Mn into the spinel [27,28].

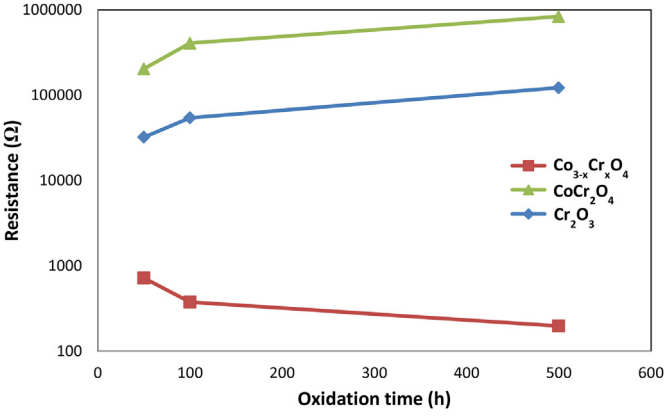

Fig. 9. Resistance measured for the oxide scales after different oxidation times.

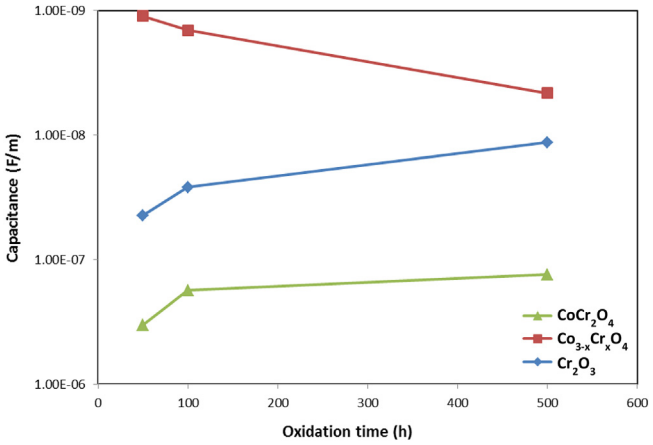

Fig. 10. Capacitance measured for the oxide scales after different oxidation times.

3.3. Estimation of the $CoCr_2O_4$ spinel layer thickness as a function of oxidation time

The growth of the $CoCr_2O_4$ spinel layer is not clearly evident in the cross-section of the oxidation samples except for the 500-h sample due to the unique thickness and compositional features of this layer. Assuming that the resistivity ρ of the $CoCr_2O_4$ spinel layer is a material property that does not change with the Cr content in it and is relatively constant irrespective of the oxidation time, the thickness of the $CoCr_2O_4$ spinel layer, l, for the other oxidation times could be estimated with the equation $\rho = RA/l$. Using the resistivity ρ of the $CoCr_2O_4$ spinel layer calculated with its resistance R measured from its impedance spectrum as well as its thickness for the 500-h sample, the thickness of the $CoCr_2O_4$ spinel layer for the other samples can be readily obtained.

Fig. 11 shows the estimated thickness of the $CoCr_2O_4$ spinel layer as a function of oxidation time. The curve can be fitted to yield a parabolic relation between the $CoCr_2O_4$ spinel layer thickness (l) and oxidation time (t), i.e., $l = \sqrt{0.0049t}$. This equation in combination with the amount of Co reservoir available in the $Co_{3-x}Cr_xO_4$ layer could be used to roughly predict the spinel layer thickness for different oxidation times. Certainly, once the $Co_{3-x}Cr_xO_4$ layer is completely consumed, the calculation will cease to be valid.

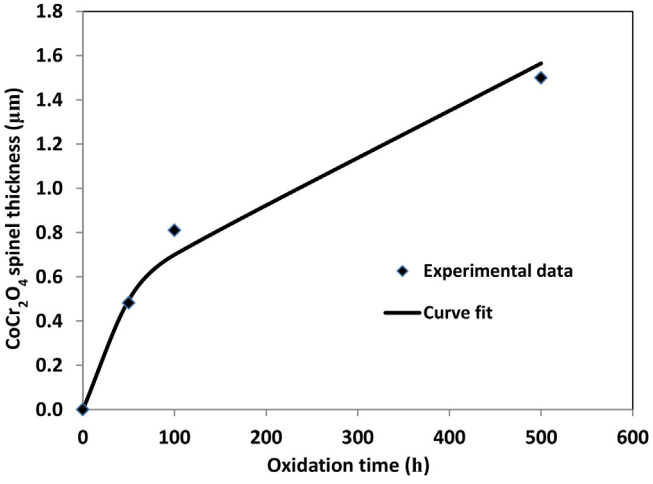

Fig. 11. Calculated thickness of the $CoCr_2O_4$ spinel layer as a function of oxidation time.

Interestingly, with the Mn addition to the Co_3O_4 to form $(Co,Mn)_3O_4$ surface layer, the formation of such intermediate layer of $CoCr_2O_4$ is either delayed or not observed [11,27,28], indicating the beneficial effect of Mn in stabilizing the surface spinel layer. However, whether a thin intermediate layer is present or completely absent between $(Co,Mn)_3O_4$ and Cr_2O_3 in such a case needs to be further studied utilizing the impedance spectroscopic approach, similar to what is reported in this paper. It should be noted that with the addition of Mn into the spinel, its electrical conductivity is also improved [29]. Furthermore, our recent work has demonstrated the feasibility of achieving a $(Co,Mn)_3O_4$ coating on the ferritic alloy substrate via the electrodeposition approach [30].

4. Conclusions

The oxide films formed on cobalt-coated Crofer 22 APU ferritic steel during oxidation at 800 °C in air for various exposure times were examined by means of impedance spectroscopy in conjunction with SEM/EDS and XRD. While the oxide films were composed of the dual Co_3O_4 and Cr_2O_3 layers for the 2-h sample, an additional $CoCr_2O_4$ spinel layer was formed between the surface spinel layer and the inner Cr_2O_3 scale for the other samples, which increased in thickness with the increase in oxidation time. Deterioration of the surface spinel layer was evident with the growth of the intermediate $CoCr_2O_4$ layer for the 500-h sample. The electrical properties of all the individual layers were obtained from the impedance data. Obviously, the Co_3O_4 coating studied in this paper is not very promising for long-term SOFC stack operation. The stability of the surface spinel layer needs to be improved and its detrimental interaction with the Cr_2O_3 scale has to be mitigated, which might be accomplished via the addition of Mn in the spinel to form the $(Co,Mn)_3O_4$ coating.

Acknowledgment

This research was supported by the Center for Manufacturing Research, Tennessee Technological University. Part of the research was also sponsored by NSF under DMR-0238113.

References

[1] J.W. Fergus, Solid State Ionics 171 (2004) 1–15.
[2] W.J. Quadakkers, J. Piron-Abellan, V. Shemet, L. Singheiser, Mater. High Temp. 20 (2003) 115–127.
[3] Z. Yang, K.S. Weil, D.M. Paxton, J.W. Stevenson, J. Electrochem. Soc. 150 (2003) A1188–A1201.
[4] W.Z. Zhu, S.C. Deevi, Mater. Res. Bull. 38 (2003) 957–972.
[5] M.C. Tucker, G.Y. Lau, C.P. Jacobson, L.C. DeJonghe, S.J. Visco, J. Power Sources 171 (2007) 477–482.
[6] P. Kofstad, R. Bredesen, Solid State Ionics 52 (1992) 69–75.
[7] K. Hilpert, D. Das, M. Miller, D.H. Peck, R. Weiß, J. Electrochem. Soc. 143 (1996) 3642–3647.
[8] H. Yokokawa, T. Horita, N. Sakai, K. Yamaji, M.E. Brito, Y.-P. Xiong, H. Kishimoto, Solid State Ionics 177 (2006) 3193–3198.
[9] T. Horita, Y.-P. Xiong, H. Kishimoto, K. Yamaji, M.E. Brito, H. Yokokawa, J. Electrochem. Soc. 157 (2010) B614–B620.
[10] L. Singheiser, J. Piron-Abelan, V. Shemet, W.-J. Quadakkers, VDI Ber. 1680 (2002) 267–274.
[11] Z.G. Yang, G.G. Xia, S.P. Simner, J.W. Stevenson, J. Electrochem. Soc. 152 (2005) A1896–A1901.
[12] Z.H. Bi, J.H. Zhu, J.L. Batey, J. Power Sources 195 (2010) 3605–3611.
[13] W. Huang, S. Gopalan, U.B. Pal, S.N. Basu, J. Electrochem. Soc. 113 (2008) 405–411.
[14] Z.H. Bi, J.H. Zhu, S.W. Du, Y.T. Li, Surf. Coat. Technol. 228 (2013) 124–131.
[15] K. Huang, P.Y. Hou, J.B. Goodenough, Mater. Res. Bull. 36 (2001) 81–95.
[16] A.N. Hansson, S. Linderoth, M. Mogensen, M.A.J. Somers, J. Alloys Compd. 433 (2007) 193–201.
[17] H. Ebrahimifar, M. Zandrahimi, Surf. Coat. Technol. 206 (2011) 75–81.
[18] X. Deng, P. Wei, M.R. Bateni, A. Petric, J. Power Sources 160 (2006) 1225–1229.
[19] Y. Larring, T. Norby, J. Electrochem. Soc. 147 (2000) 3251–3256.
[20] E. Barsoukov, J.R. MacDonald, Impedance Spectroscopy: Theory, Experiment, and Applications, second ed., Wiley-Interscience, 2005.
[21] G.V. Samsonov (Ed.), The Oxide Handbook, IFI Plenum, New York, 1973.
[22] T. Jacobsen, B. Zachau-Christiansen, L. Bay, S. Skaarup, in: F.W. Paulsen, N. Bonanos, S. Linderoth, M. Mogensen, B. Zachau-Christiansen (Eds.), Proceedings of the 17th Risø International Symposium on Materials Science, "High Temperature Electrochemistry: Ceramics and Metals", Risø National Laboratory, Roskilde, Denmark, 1996, p. 29.
[23] S.-H. Song, P. Xiao, J. Mater. Sci. 38 (2003) 499–506.
[24] N.K. Appandairajan, J. Gopalakrishnan, Proc. Indian Acad. Sci. Sect. A 87 (1978) 115.
[25] A.N. Hansson, S. Linderoth, M. Mogensen, M.A.J. Somers, J. Alloys Compd. 402 (2005) 194–200.
[26] W. Qu, L. Jian, J.M. Hill, D.G. Ivey, J. Power Sources 153 (2006) 114–124.
[27] J.W. Fergus, Y. Liu, Y. Zhao, Ceram. Trans. 236 (2012) 141–145.
[28] J.W. Stevenson, Z.G. Yang, G.G. Xia, Z. Nie, J.D. Templeton, J. Power Sources 231 (2013) 256–263.
[29] A. Petric, H. Ling, J. Am. Ceram. Soc. 90 (2007) 1515–1520.
[30] M.J. Lewis, J.H. Zhu, Electrochem. Solid-State Lett. 14 (2011) B9–B12.